
Thermal slip effect on MHD convective nanofluid flow over a vertical plate embedded in a porous medium

K. Swain^{1,*}, S. K. Parida², G. C. Dash²

1. Department of Mathematics, Radhakrishna Institute of Technology and Engineering, Bhubaneswar, 752057, India

2. Department of Mathematics, Siksha 'O' Anusandhan (Deemed to be University), Bhubaneswar, 751030, India

kharabela1983@gmail.com

ABSTRACT. In the present analysis contributions of viscous and Ohmic dissipations on a MHD convective nanofluid flow with thermal slip are studied. Further, the effects of thermal radiation, permeability of the medium in the presence of heat source/sink are also analysed. The numerical solutions to governing equations are obtained applying fourth order Runge-Kutta method with an error tolerance of 10^{-4} . The velocity, temperature, concentration and nanoparticle volume fraction profiles are presented graphically. The surface criteria in respect of shearing stress and rate of heat transfer are also discussed. The validation of the reported results complements to the observations. One striking outcome is to note that the presence of sink causes heat flow from the fluid to bounding surface. This may be ascribed to significant generation of heat due to viscous and Ohmic dissipations in nanofluid flow to override the effect of sink.

RÉSUMÉ. On étudie les contributions des dissipations visqueuses et ohmiques sur un flux de nanofluides convectifs MHD avec un glissement thermique. Par ailleurs, les effets du rayonnement thermique, la perméabilité du milieu en présence de source de chaleur / puits sont également analysés. Les solutions numériques aux équations sont acquises tout en appliquant la méthode de Runge-Kutta classique d'ordre quatre (RK4) avec une tolérance aux pannes de 10^{-4} . Les profils de vitesse, de température, de concentration et de fraction de volume de nanoparticules sont présentés de façon graphique. Les critères de surface concernant la contrainte de cisaillement et le ratio de transfert de chaleur sont également discutés. La validation des résultats rapportés résulte d'un complément des observations. Un résultat remarquable mérite notre attention. Il est à noter que la présence d'un évier provoque un flux de chaleur du fluide tournant vers la surface délimitée. Cela peut être attribué à une génération importante de la chaleur due à des dissipations visqueuses et ohmiques dans un flux de nanofluide pour outrepasser l'effet de l'évier.

KEYWORDS: MHD, nanofluid, Joule heating, radiation, viscous dissipation, porous medium.

MOTS-CLÉS: MHD, nanofluide, effet Joule, radiation, dissipation visqueuse, milieu poreux.

DOI:10.3166/EJEE.20.215-233 © 2018 Lavoisier

1. Introduction

The nanofluids are of immense use in many industrial and technological applications such as melt polymers, electronic-cooling, solar collectors, biological solutions, food mixing and nuclear reactors because of their increasing thermal conductivity property, stability and homogeneity. Usually fluids such as water, ethylene glycol and mineral salts are used in heat transfer process as base fluid and exhibit low thermal conductivity without nanoparticle. Choi *et al.* (2001) pointed out that the effect of a small amount of nanoparticles added to any standard fluid (less than one percent by volume) enhances, approximately twice, the thermal conductivity property of the base fluid. Buongiorno (2006) developed a nanofluid model considering Brownian diffusion and thermophoresis slip mechanism.

The slip flow usually occurs in small-characteristic-size flow system or flow under very low pressure. The slip may occur on a stationary and moving boundary when the fluid is particulate such as emulsions and suspensions. To account for the slip at the boundary, Navier (1823) incorporated a boundary condition where the component of tangential fluid velocity to the boundary walls is directly related to tangential stress. Kuznetsov and Nield (2014) studied analytically the natural convective boundary layer nanofluid flow past a vertical plate. They have considered the effects of thermophoresis and Brownian motion.

The scattering of mass because of temperature gradient is called Soret or thermo-diffusion effects and this effect is significant in case of large density differences between the fluid layers. For instance, when a species of lower density than that of the surrounding fluid, is introduced into the flow then Soret effect arises. This finds application in separation of isotopes. The Soret and Dufour effect on mixed convection heat and mass transfer are studied by Pal and Chatterjee (2014), Srinivasacharya and RamReddy (2011). Makinde and Aziz (2011) studied numerically boundary layer flow of a nanofluid past a stretching sheet subject to a convective thermal boundary condition. Turkyilmazoglu (2013) studied the Soret and Dufour effect on MHD flow of an electrically conducting viscoelastic fluid past a vertical stretching surface in a porous media.

Usually nanofluids are electrically conducting due to presence of nanoparticles. Therefore, flowing nanofluids produce electromagnetic resistive force under the influence of externally applied magnetic field. Rama and Goyal (2014) investigated non-Newtonian nanofluid flow over a permeable sheet with heat generation and velocity slip in presence of magnetic field. Yadav *et al.* (2015) also studied the impact of internal heating on conducting nanofluid. Chandrasekhar and Rudraiah (1980) have analyzed the effect of uniform transverse magnetic field on the flow behavior of viscous conducting fluid in a channel with non-uniform gap. Pal and Mandal (2014) investigated the mixed convection boundary layer flow of nanofluid at a stagnation point over a permeable stretching/shrinking sheet. Ahmad and Khan (2015) reported the unsteady incompressible MHD water-based nanofluid flow considering Buongiorno model.

The boundary layer flow is governed by two transport mechanism i.e. momentum transport which gives rise to velocity boundary layer and heat transport which contributes to the growth of thermal boundary layer. Recently, Ram Reddy *et al.* (2013) studied the Soret effect on mixed convection flow in a nanofluid subject to convective boundary condition. Despite their interesting analysis, they have not considered the following aspects.

- (i) The permeability of the saturated porous medium which modifies the momentum equation with an additional body force per unit mass and finds application in geothermal and geophysical problems.
- (ii) Viscous dissipation, a measure of rate of doing work due to viscous resistance. Julian dissipation, the dissipation of electromagnetic energy (Joule heating).
- (iii) Thermal radiation.
- (iv) Volumetric heat source which can be created by electrical devices or otherwise.

The inclusion of the above criteria modifies the thermal as well as velocity boundary layer equations. Under the present study, consideration of Soret effect i.e. mass diffusion due to temperature gradient is justified as the nanoparticle gets diffused to the base fluid. Most appropriately, the consideration of thermal slip at the boundary warrants that the mean free path is not negligible when compared with the dimensions of the body in the flow domain (Pai, 1959).

2. Mathematical model and flow analysis

Consider the steady laminar two dimensional flow of a viscous incompressible nanofluid over a semi-infinite vertical plate embedded in a porous medium. Cartesian co-ordinate system is shown in Figure 1. The ambient temperature, concentration and volume fraction are shown in Figure 1 as T_∞ , C_∞ , and ϕ_∞ respectively. The plate is heated/cooled depending upon $T_f < T_\infty$ or $T_f > T_\infty$, where T_f is the fluid temperature.

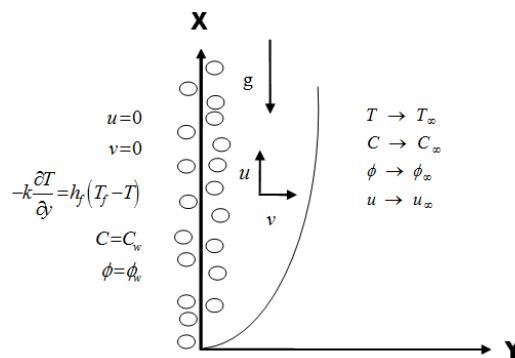


Figure 1. Flow configuration

The governing equations for the nanofluid flow with Oberbeck-Boussinesq approximation which is a two part approximation, which neglects all variable properties in the governing equations except the density in the buoyancy term of momentum equation and approximate the density difference with a simplified equation of state i.e. $\rho = \rho_\infty [1 - \beta_T (T - T_\infty)]$ (similar term for concentration). Following RamReddy *et al.*, governing equations are given by

$$\frac{\partial u}{\partial x} + \frac{\partial v}{\partial y} = 0 \tag{1}$$

$$\rho_{f_\infty} \left(u \frac{\partial u}{\partial x} + v \frac{\partial u}{\partial y} \right) = \mu \frac{\partial^2 u}{\partial y^2} + g \rho_{f_\infty} (1 - \phi_\infty) \left[\begin{matrix} \beta_T (T - T_\infty) + \\ \beta_C (C - C_\infty) \end{matrix} \right] - (\rho_p - \rho_{f_\infty}) g (\phi - \phi_\infty) - \sigma B_0^2 u - \frac{\mu}{K_p} u \tag{2}$$

$$\frac{\partial T}{\partial t} + u \frac{\partial T}{\partial x} + v \frac{\partial T}{\partial y} = \alpha_m \frac{\partial^2 T}{\partial y^2} + \frac{1}{\rho_{f_\infty} c_p} \left[\frac{\partial}{\partial y} \left(\frac{\partial T}{\partial y} \right) \right] \tag{3}$$

$$\frac{\partial C}{\partial t} + u \frac{\partial C}{\partial x} + v \frac{\partial C}{\partial y} = D \frac{\partial^2 C}{\partial y^2} \tag{4}$$

$$\frac{\partial \phi}{\partial t} + u \frac{\partial \phi}{\partial x} + v \frac{\partial \phi}{\partial y} = \tau \frac{\partial^2 \phi}{\partial y^2} \tag{5}$$

where u and v are components of velocity along x and y axes respectively, T is the temperature, ϕ is the nanoparticle volume fraction, C is the solutal concentration, g is the acceleration due to gravity, $\alpha_m = \frac{k}{(\rho c)_f}$ is the thermal diffusivity of the fluid, $\nu = \frac{\mu}{\rho_{f_\infty}}$ is the kinematic viscosity coefficient and $\tau = \frac{(\rho c)_p}{(\rho c)_f}$ is the ratio of the effective heat capacity of the nanoparticle material and the fluid.

The above governing equations are consistent with the assumptions that (i) the solid matrix is everywhere in local thermodynamic equilibrium, (ii) the thermo physical properties of the fluid are homogeneous and isotopic, and (iii) there is a thermal slip on the bounding surface.

The boundary conditions for the thermal field may be prescribed following Aziz (2009) as

$$\begin{aligned}
 y = 0 : \quad & u = 0, \quad v = 0, \quad -k \frac{\partial T}{\partial y} = h_f (T_f - T), \quad \phi = \phi_w, \quad C = C_w \\
 y \rightarrow \infty : \quad & u \rightarrow u_\infty, \quad T \rightarrow T_\infty, \quad \phi \rightarrow \phi_\infty, \quad C \rightarrow C_\infty
 \end{aligned}
 \tag{6}$$

By using the following similarity transformations

$$\begin{aligned}
 \eta = \frac{y}{\sqrt{2x}} \operatorname{Re}_x^{1/2}, \quad f(\eta) = \frac{1}{\sqrt{2\nu}} \operatorname{Re}_x^{-1/2} \psi(\eta), \\
 \theta(\eta) = \frac{T - T_\infty}{T_w - T_\infty}, \quad \gamma(\eta) = \frac{\phi - \phi_\infty}{\phi_w - \phi_\infty}, \quad S(\eta) = \frac{C - C_\infty}{C_w - C_\infty}
 \end{aligned}$$

with stream function $\psi(x,y)$ such that $u = \frac{\partial \psi}{\partial y}$ and $v = \frac{\partial \psi}{\partial x}$

the equations (2) - (5) and boundary conditions (6) reduce to

$$f''' + ff'' - \left(M + \frac{1}{K_p} \right) f' + 2\lambda [\theta + NcS - Nr\gamma] = 0
 \tag{7}$$

$$\left(1 + \frac{4}{3}R \right) \theta'' + \operatorname{Pr} \left[f\theta' + Nb\theta'\gamma' + Nt\theta'^2 + Ec \left\{ (f'')^2 + M(f')^2 \right\} + Q\theta \right] = 0
 \tag{8}$$

$$\gamma'' + Lef\gamma' + \frac{Nt}{Nb} \theta'' = 0
 \tag{9}$$

$$S'' + S_r Le \operatorname{Pr} \theta'' + Le \operatorname{Pr} f S' = 0
 \tag{10}$$

$$\left. \begin{aligned}
 \eta = 0 : \quad & f(0) = 0, \quad f'(0) = 0, \quad \theta'(0) = -Bi[1 - \theta(0)], \\
 & \gamma(0) = 1, \quad S(0) = 1 \\
 \eta \rightarrow \infty : \quad & f'(\infty) \rightarrow 1, \quad \theta(\infty) \rightarrow 0, \quad \gamma(\infty) \rightarrow 0, \quad S(\infty) \rightarrow 0
 \end{aligned} \right\}
 \tag{11}$$

where non-dimensional variables and parameters are

$$\begin{aligned}
 M &= \frac{2\sigma B_0^2 x}{\rho_{f\infty} u_\infty}, K_p = \frac{K_p^* u_\infty}{2\nu x}, Q = \frac{2Q_0 x}{u_\infty}, Pr = \frac{\nu}{\alpha_m}, \\
 Le &= \frac{\alpha_m}{D_B}, Ec = \frac{u_\infty^2}{C_p (T_f - T_\infty)}, Re_x = \frac{u_\infty x}{\nu}, \\
 Nb &= \frac{(\rho c)_p D_B (\phi_w - \phi_\infty)}{(\rho c)_f \nu}, Nc = \frac{\beta_C (C_w - C_\infty)}{\beta_T (T_f - T_\infty)}, \\
 Nr &= \frac{(\rho_p - \rho_{f\infty})(\phi_w - \phi_\infty)}{\rho_{f\infty} \beta_T (T_f - T_\infty)(1 - \phi_\infty)}, R = \frac{4\sigma^* T_\infty^3}{kk^*}, \\
 S_T &= \frac{D_{CT} (T_f - T_\infty)}{\nu (C_w - C_\infty)}, Nt = \frac{(\rho c)_p D_T (T_f - T_\infty)}{(\rho c)_f \nu T_\infty}, \\
 \lambda &= \frac{Gr_x}{Re_x^2}, Gr_x = \frac{g \beta_T (1 - \phi_\infty)(T_f - T_\infty) x^3}{\nu^2}
 \end{aligned}$$

and $B_i = \frac{c}{k} \sqrt{\frac{2\nu}{u_\infty}}$ is the Biot number. This boundary condition will be free from the local variable x by choosing $h_f = cx^{-1/2}$.

3. Skin friction, heat and mass transfer coefficients

The shearing stress, local heat transfer, local nanoparticle mass and local regular mass fluxes at the vertical plate can be obtained from

$$\begin{aligned}
 \tau_w &= \mu \left[\frac{\partial u}{\partial y} \right]_{y=0}, \quad q_w = -k \left[\frac{\partial T}{\partial y} \right]_{y=0}, \quad q_m = -D_s \left[\frac{\partial C}{\partial y} \right]_{y=0} \quad (12) \\
 q_n &= -D_B \left[\frac{\partial \phi}{\partial y} \right]_{y=0}
 \end{aligned}$$

The non dimensional shear stress coefficient $C_f = \frac{\tau_w}{\rho_{f\infty} u_\infty^2}$, the Nusselt number $N_{u_x} = \frac{q_w x}{k(T_f - T_\infty)}$, the nanoparticle Sherwood number $NSH_x = \frac{q_n x}{D_B(\phi_w - \phi_\infty)}$ and the regular Sherwood number $Sh_x = \frac{q_m x}{D_s(C_w - C_\infty)}$, are given by

$$C_f = \frac{f''(0)}{(2\text{Re}_x)^{1/2}}, Nu_x = -\left(\frac{\text{Re}_x}{2}\right)^{1/2} \theta'(0),$$

$$NSh_x = -\left(\frac{\text{Re}_x}{2}\right)^{1/2} \gamma'(0), Sh_x = -\left(\frac{\text{Re}_x}{2}\right)^{1/2} S'(0)$$

4. Results and discussion

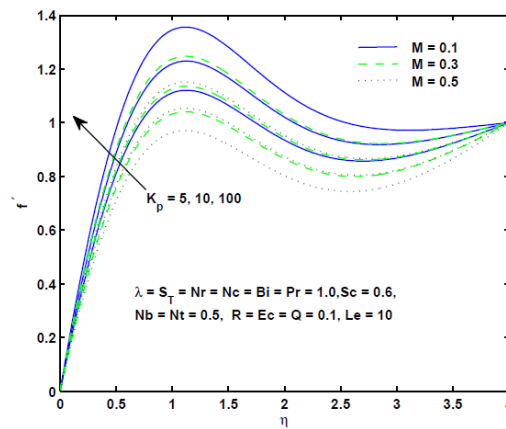


Figure 2. Effects of M and KP on velocity profiles

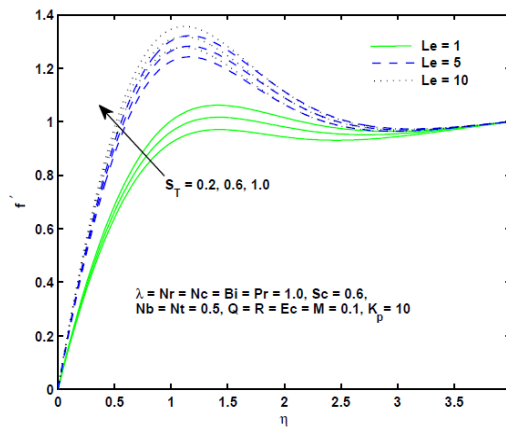


Figure 3. Effects of St and Le on velocity profiles

The non-linear ordinary differential equations (7) - (10) with boundary conditions (11) have been solved using Runge-Kutta fourth order method with a self-corrective and iterative procedure i.e. shooting technique. The present mixed convective flow model is a generalization of Makinde and Olanrewaju (2010), Subhashini *et al.* (2011) and RamReddy *et al.* (2013).

Figures 2 and 5 exhibit the effect of magnetic parameter (M) and porosity parameter (K_p) on velocity and temperature distributions respectively. The interaction of magnetic field with an electrically conducting flowing fluid induces a voltage across the magnetic field. The current generated by the induced voltage interacts with magnetic field and produces a resistive force to slow down the motion of the fluid (Cramer and Pai, 1973). Therefore, an increase in M leads to decrease the velocity and enhances the thermal energy giving rise to higher temperature profile (Figure 5). Further, porous medium resists the fluid flow also. The temperature distribution is asymptotic in nature showing a good agreement with prescribed ambient temperature. On careful observation of velocity profiles it reveals that velocity boundary layer develops flow instability for $\eta=2.25$ (approx.), and it is more pronounced for higher value of M , due to appearance of inflexion point at $\eta=2.25$. Hence, it is concluded that induced electromagnetic force gives rise to thinner velocity boundary layer and thicker thermal boundary layer owing to reduction of velocity and rise in temperature respectively.

From figure 3, it is seen that the momentum boundary layer thickness increases with the increase in Lewis number (Le) as well as Soret number. The Lewis number is a relative measure of kinematic viscosity and Brownian diffusivity. An increase in Lewis number enhances the kinematic viscosity of the fluid, consequently accelerating the momentum transfer in the boundary layer leading to increase in velocity. In case of Soret number, Soret diffusivity coupled with higher temperature difference between fluid and ambient temperature contribute to rise in temperature. For validity of the result of the present study, figure 3 is compared with that of Ram Reddy *et al.* It is observed that the profiles exhibit similar characteristics for $S_T=0.2, 1.0$ and $Le=1, 10$. This is a particular case of agreement setting aside the other Figures which also exhibit the same phenomena in respect of other parameters.

From figure 4 it is evident that an increase in Biot number (B_i) and mixed convection parameter (λ) enhance the velocity. The Biot number is the ratio of momentum diffusivity through ν and thermal diffusivity through k . Here, momentum diffusivity is accelerated overriding the thermal conductivity of nanofluid, resulting accelerated fluid motion.

Figure 6 illustrates the effects of Brownian motion (Nb) and thermophoresis parameter Nt on temperature profiles. An increase in both Nb and Nt which leads to increase the temperature indicating more diffusion of thermal energy in to the flow domain. As we have defined the parameters Nb and Nt it is evident that those exhibit the physical properties: such as solutal and thermal differences, Brownian diffusivity, ratio of specific heat capacities of nanoparticle and fluid particle. It is revealed that thermal energy is dissipated into flow due to concentration and temperature

differences between boundary layers and corresponding ambient conditions as well as Brownian diffusion coefficient and thermophoresis.

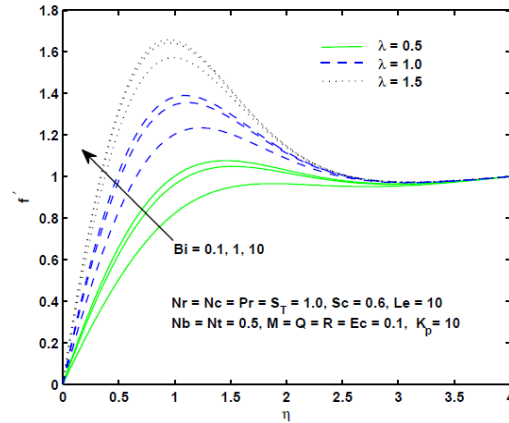


Figure 4. Effects of B_i and λ on velocity profiles

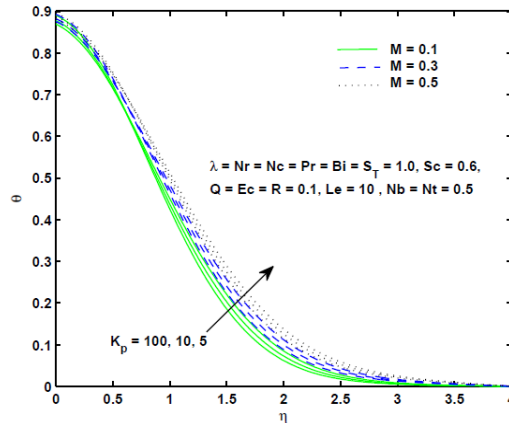


Figure 5. Effects of M and K_p on temperature profiles

Figure 7 presents the effect of variations of Prandtl number (Pr) and Biot number (B_i) on the fluid temperature. A fluid with higher Prandtl number has a relatively lower thermal diffusion, resulting a decrease of temperature of the common fluid without nanoparticle. It is interesting to note that the presence of nanoparticle has enhanced the fluid temperature of low conductive fluid which is the main objective of the present study. The case of $Pr=1$ represents the equality of momentum diffusivity and thermal diffusivity resulting the coincidence of both velocity and thermal boundary layers.

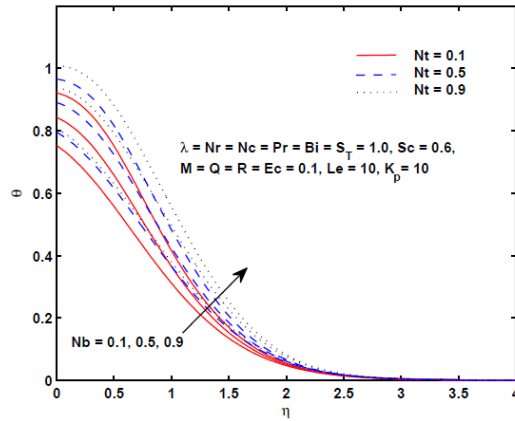


Figure 6. Effects of N_b and N_t on temperature profiles

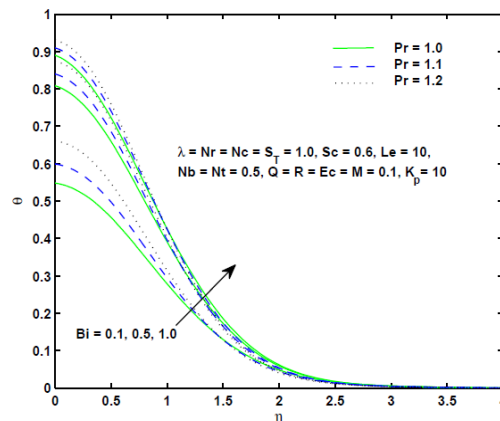


Figure 7. Effects of P_r and B_i on temperature profiles

Figure 8 shows the effect of heat source/sink (Q) and Eckert number (Ec) on the temperature profiles. Both the parameters enhance the temperature. The Eckert number measures the energy dissipated due to work done to overcome the viscous resistance and to produce heat energy to enhance the temperature in the flow domain.

From figure 9, it is seen that both radiation parameter R and mixed convection parameter (λ) decelerate the temperature in the region far off the bounding surface at $\eta=1$ but the reverse effect is observed in the region close to the boundary. This shows a transition in variation of temperature occurs due to mixed convection and thermal radiation. The radiation effect in case of high temperature gradient and thermal slip

on the bounding surface are accounted for in the present study. Both the conditions exert their effects in the layers close to the bounding surface.

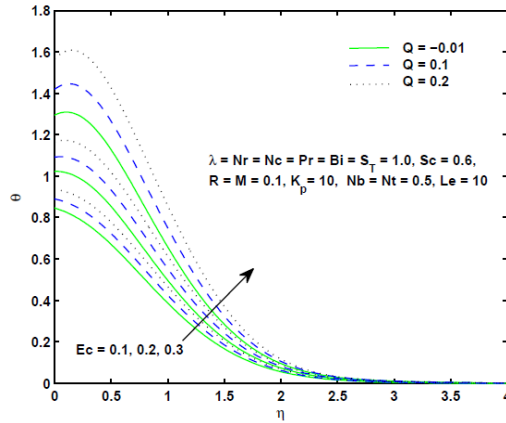


Figure 8. Effects of Q and Ec on temperature profiles

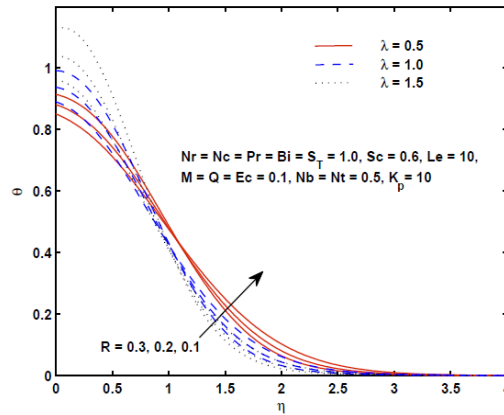


Figure 9. Effects of λ and R on temperature profiles

Figure 10 exhibits the effect of Soret number (S_T), affecting the diffusion of mass due to temperature gradient and Sc , ratio of kinematic viscosity and solutal diffusivity (Sc). The higher Sc representing heavier species which lowers down the concentration level in all the layers whereas, reverse effect is observed in case of Soret number. The increase in S_T is the outcome of increase in fluid temperature difference and Soret diffusivity coefficient resulting a rise in concentration level.

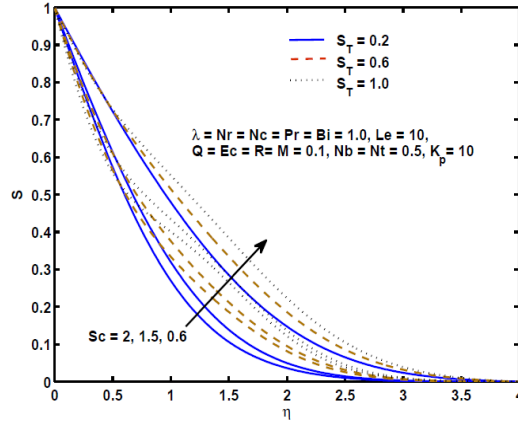


Figure 10. Effects of S_r and S_c on concentration profiles

Figure 11 displays the effects of regular buoyancy ratio (N_c) and nanoparticle buoyancy ratio (N_r) on concentration profiles. It is seen that nanofluid buoyancy ratio commensurate with the concentration level where as regular buoyancy ratio acts adversely. This shows that the presence of nanoparticle not only enhances the thermal energy level but also concentration in the flow domain.

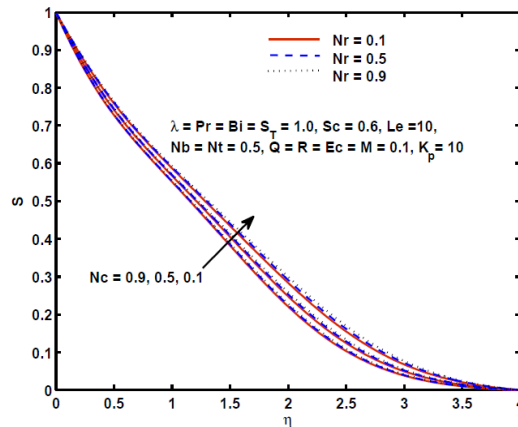


Figure 11. Effects of N_c and N_r on concentration profiles

From figure 12, it is evident that Lewis number and mixed convection parameter both reduce the volume fraction in the nanofluid flow. One striking feature of the profile is that Le has a significant effect on volume fraction. For the high values of Le equal to 5 and 10, the volume fraction decreases sharply where as for $Le=1$, slow and uniform decrease is indicated.

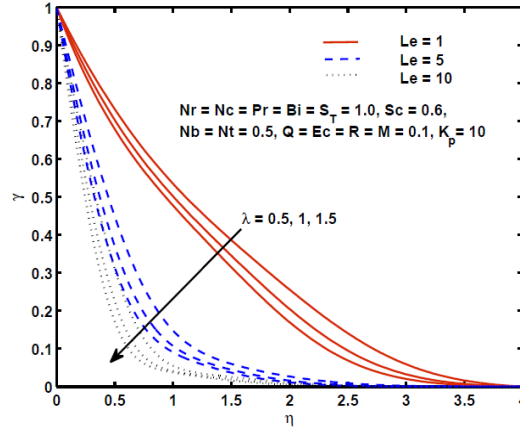


Figure 12. Effects of λ and Le on volume fraction profiles

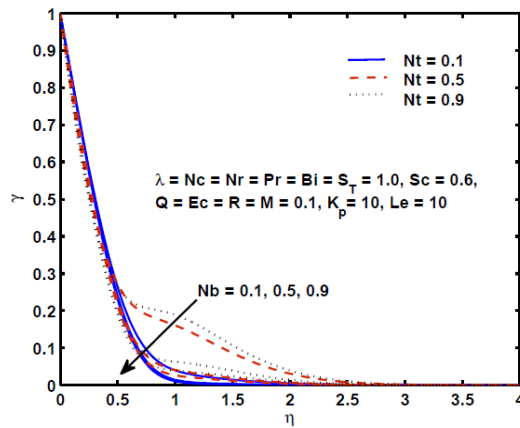


Figure 13. Effects of Nb and Nt on volume fraction profiles

Figure 13 illustrates the effects of Brownian motion (Nb) and thermophoresis parameter (Nt) on volume fraction profiles. A sharp fall in volume fraction is seen with the variation of Nb and Nt barring some anomalies in case of slightly increased value of Nt equals to 0.5, 0.9. The fall of volume fraction slows down for $0.6 < \eta < 1.9$. This indicates that increase in Brownian motion prevents higher energy exchange. Further, it is seen that the increase in Le , due to rise in thermophoresis, prevents the reduction of volume fraction.

To check the accuracy of the numerical method, the values of $f'(0)$ and $-\theta'(0)$ are compared with RamReddy *et al.*, Makinde and Olanrewaju (2010) and Subhashini *et*

al. (2011) in Table 1 and are found to be in good agreement.

Table 1. Comparison of $f'(0)$ and $-\theta'(0)$ for various values of Bi, λ, Pr

Bi	λ	Pr	Makinde and Olanrewaju (2010)		Subhashini et al. (2011)		RamReddy et al. (2013)		Present Study	
			$f'(0)$	$-\theta'(0)$	$f'(0)$	$-\theta'(0)$	$f'(0)$	$-\theta'(0)$	$f'(0)$	$-\theta'(0)$
0.1	0.1	0.7	0.36881	0.07507	0.36875	0.07505	0.36898	0.07509	0.36877	0.07580
1.0	0.1	0.7	0.44036	0.23750	0.44032	0.23746	0.44049	0.23765	0.44171	0.23859
0.1	1.0	0.7	0.63200	0.07704	0.63198	0.07700	0.63197	0.07705	0.63195	0.07717
0.1	0.1	3.0	0.34939	0.08304	0.34937	0.08301	0.34957	0.08308	0.34801	0.08405
0.1	0.1	7.1	0.34270	0.08672	0.34270	0.08670	0.34289	0.08674	0.34265	0.08620

Table 2 presents the skin friction coefficients, rates of heat transfer, nanoparticle mass transfer, regular mass transfer for different values of the Soret number (S_T), Lewis number (Le), Biot number (Bi), heat source/sink (Q). It is observed that all these surface criteria, increase with S_T, Le, Bi, Q but decrease with the increasing values of magnetic parameter (M) and nanoparticle buoyancy ratio Nr . Some specific observations are laid down as:

Table 2. Values of skin friction coefficients, heat, nanoparticle mass and regular mass transfer rates for various values of S_T, Le, Bi, Nr, M and Q when $Nc=Pr=\lambda=1.0, Nb=Nt=0.5$ and $Sc=0.6$

S_T	Le	Bi	Nr	M	Q	$f'(0)$	$-\theta'(0)$	$-S'(0)$	$-r'(0)$
0.2	1.0	1.0	1.0	0	0	1.637782	0.128809	0.500225	0.564563
0.2	1.0	1.0	1.0	0	-0.2	1.499453	0.016111	0.480990	0.490874
0.2	1.0	1.0	1.0	0	0.1	1.718198	0.190961	0.511221	0.607181
0.2	1.0	1.0	1.0	0	0.2	1.807602	0.258056	0.523294	0.654426
0.2	1.0	1.0	1.0	0.1	0.2	1.798612	0.257579	0.522028	0.653207
0.2	1.0	1.0	1.0	0.5	0.2	1.614710	0.247029	0.494539	0.628525
0.2	1.0	1.0	1.0	1.0	0.2	1.303619	0.227553	0.439203	0.583739

0.4	1.0	1.0	1.0	1.0	0.2	1.307754	0.228142	0.446535	0.584779
1.0	1.0	1.0	1.0	1.0	0.2	1.322571	0.230018	0.446296	0.588282
1.0	1.0	1.0	1.0	1.0	0.2	1.774123	0.332384	0.518168	1.599425
1.0	100	1.0	1.0	1.0	0.2	2.036420	0.533254	0.532938	3.633789
1.0	100	10	1.0	1.0	0.2	2.238490	0.669274	0.552316	3.764444
1.0	100	20	1.0	1.0	0.2	2.252150	0.678531	0.553697	3.773173
1.0	100	20	0.5	1.0	0.2	2.387944	0.684565	0.555893	3.821201
1.0	100	20	0.1	1.0	0.2	2.494677	0.698877	0.554634	3.852858

Table 3. Verification of skin friction coefficients, heat, nanoparticle mass and regular mass transfer rates for various values of Nb , Nt , λ , Nc , M and Q when $Nr=Pr=Bi=S_T=1.0$, $Le=10$ and $Sc=0.6$

Nb	Nt	λ	Nc	M	Q	$f''(0)$	$-\theta'(0)$	$-S'(0)$	$-r'(0)$
0.1	0.1	1.0	1.0	0	0	2.222133	0.078336	0.473591	1.624380
0.1	0.1	1.0	1.0	0	-0.2	2.154676	-0.030159	0.444414	1.575723
0.1	0.1	1.0	1.0	0	0.1	2.261109	0.137492	0.490673	1.652582
0.1	0.1	1.0	1.0	0	0.2	2.304310	0.200498	0.508641	1.681904
0.1	0.1	1.0	1.0	0.1	0.2	2.293675	0.200376	0.507656	1.679080
0.1	0.1	1.0	1.0	0.5	0.2	2.065333	0.197750	0.485660	1.615801
0.1	0.1	1.0	1.0	1.0	0.2	1.603554	0.192622	0.437091	1.468463
0.5	0.1	1.0	1.0	1.0	0.2	1.719824	0.326281	0.495968	1.504821
0.9	0.1	1.0	1.0	1.0	0.2	1.812047	0.392078	0.545419	1.529423
0.9	0.5	1.0	1.0	1.0	0.2	1.868138	0.375751	0.565924	1.610361
0.9	0.9	1.0	1.0	1.0	0.2	1.926220	0.355756	0.583878	1.695506
0.9	0.9	2.0	1.0	1.0	0.2	3.330341	0.479635	0.663230	2.017345
0.9	0.9	3.0	1.0	1.0	0.2	4.557491	0.570684	0.721140	2.231159
0.9	0.9	3.0	2.0	1.0	0.2	7.022099	0.707463	0.808529	2.542765
0.9	0.9	3.0	3.0	1.0	0.2	9.287668	0.819497	0.874428	2.772878

- (i) Positive values of $-\theta'(0)$ show that the heat flows from bounding surface to the fluid.
- (ii) The rates of change remain positive in the presence/absence of heat source and sink.

(iii) The presence of magnetic field, nanoparticle reduce the surface conditions particularly skin friction so that it enforces the stability of the flow.

Table 3 presents the same surface conditions (rate coefficients) as in Table 2 for Brownian motion parameter (Nb), mixed convection parameter (λ) and regular buoyancy ratio (Nc). One interesting outcome is that in the presence of heat sink, rate of heat transfer at the plate assumes negative values which indicate that the heat flows from the fluid to the wall. Rates of change at the surface indicated in Table 3 increases with the increasing values of all the parameters except the magnetic parameter having opposite effect. This interesting result admits of a physical interpretation. For assigned values of other parameters, both viscous and Ohmic dissipation in the flow are large enough to override the effect of sink and hence heat flows from the fluid to plate.

5. Conclusion

From the present study the following conclusions are drawn:

- (i) The induced electromagnetic force gives rise to thinner velocity boundary layer and thicker thermal boundary layer.
- (ii) Soret diffusivity coupled with higher temperature difference between fluid and ambient temperature contribute to rise in temperature.
- (iii) Increase in Biot number and mixed convection parameter accelerates the velocity.
- (iv) In the presence of sink, the heat flows from the fluid to bounding surface. This may be ascribed to significant heat generation due to viscous and Ohmic dissipations in nanofluid flow.
- (v) Increase in Soret number contributes to rise in solutal concentration.
- (vi) The nanofluid buoyancy ratio commensurate with the concentration level where as regular buoyancy ratio acts adversely in the flow domain.
- (vii) For higher value of Lewis number sharp fall of volume fraction is indicated.
- (viii) The increase in Lewis number favours higher exchange of energy to prevent the reduction of volume fraction.
- (ix) There is a good agreement of the present work with that of previous ones in particular a case (Table 1 and Figure 3).
- (x) Presence of magnetic field, i.e. diffusion of magnetic intensity and nanoparticles, enforce the flow stability by reducing surface criteria, particularly, the skin friction.

References

- Ahmad R., Khan W. A. (2015). Unsteady heat and mass transfer Magnetohydrodynamic (MHD) nanofluid flow over a stretching sheet with heat source-sink using quasi linearization technique. *Canadian J. of physics*, Vol. 93, No. 12, pp. 1477-1485. <https://doi.org/10.1139/cjp-2014-0080>
- Aziz A. (2009). A similarity solution for laminar thermal boundary layer over a flat plate with convective boundary condition. *Commun. Nonlinear Sci. Simul.*, Vol. 14, pp. 1064-1068. <https://doi.org/10.1016/j.cnsns.2008.05.003>
- Buongiorno J. (2006). Convective transport in nanofluids. *ASME, J. Heat Transf.*, Vol. 128, No. 3, pp. 240-250. <https://doi.org/10.1115/1.2150834>
- Chandrasekhar B. C., Rudraiah N. (1980). MHD flow through a channel of varying gap. *Int. J. Pure and applied Math.*, Vol. 11, pp. 1105-1123. [https://doi.org/10.1016/0165-0114\(80\)90027-5](https://doi.org/10.1016/0165-0114(80)90027-5)
- Choi S., Zhang Z. G., Yu W., Lockwood F. E., Grulke E. A. (2001). Anomalously thermal conductivity enhancement in nanotubes suspensions. *Applied Physics Letters*, Vol. 79, No. 14, pp. 2252-2254. <https://doi.org/10.1063/1.1408272>
- Cramer R. K., Pai S. (1973). Magnetic flow dynamics for engineering and applied physicists. *Scripta Publishing Company, Washington D.C.*, pp. 2.
- Kuznetsov A.V., Nield D. A. (2014). Natural convective boundary layer flow of a nanofluid past a vertical plate. *Int. J. Therm. Sci.*, Vol. 49, pp. 243-247.
- Makinde O. D., Aziz A. (2011). Boundary layer flow of a nanofluid past a stretching sheet with a convective boundary condition. *Int. J. Therm. Sci.*, Vol. 50, pp. 1326-1332. <https://doi.org/10.1016/j.ijthermalsci.2011.02.019>
- Makinde O. D., Olanrewaju P. O. (2010). Buoyancy effects on thermal boundary layer over a vertical plate with a convective surface boundary condition: New results. *J. Fluids Eng.*, Vol. 132, No. 7, pp. 044502-1. <https://doi.org/10.1007/s11012-015-0122-3>
- Navier C. L. M. H. (1823). Memoire sur les lois du mouvement des fluids. *Mem. Acad. Sci. Inst. Fr.*, Vol. 6, pp. 389-416.
- Pai S. (1959). Viscous flow theory, *D. Van Nostrand Company, New York*, pp. 2.
- Pal D., Chatterjee S. (2013). Soret and Dufour effects on MHD convective heat and mass transfer of a power-law fluid over an inclined plate with variable thermal conductivity in a porous medium. *Applied Mathematics and computation*, Vol. 219, No. 14, pp. 7556-7574. <https://doi.org/10.1016/j.amc.2012.10.119>
- Pal D., Mandal G. (2014). Influence of thermal radiation on mixed convection heat and mass transfer stagnation point flow in nanofluids over stretching/shrinking sheet in a porous medium with chemical reaction. *Nuclear Eng. Design*, Vol. 273, pp. 644-652. <https://doi.org/10.1016/j.nucengdes.2014.01.032>
- Rama B., Goyal M. (2014). MHD non-Newtonian nano fluid flow over a permeable stretching sheet with heat generation and velocity slip. *Int. J. Math. Comput. Phys Quantum Eng.*, Vol. 8, pp. 910-916. <https://doi.org/10.5281/zenodo.1093128>
- RamReddy C., Murthy P. V. S. N., Chamkha A. J., Rashad A. M. (2013). Soret effect on mixed convection flow in a nanofluid under convective boundary condition. *International Journal*

of *Heat and Mass Transfer*, Vol. 64, pp. 384-392.
<https://doi.org/10.1016/j.jheatmasstransfer.2013.04.032>

Srinivasacharya D., RamReddy C. (2011). Mixed convection heat and mass transfer in a non-Darcy micropolar fluid with Soret and Dufour effects. *Nonlinear Anal. Model. Contr.*, Vol. 16, pp. 100-115. <https://doi.org/10.4208/aamm.10-m1038>

Subhashini S.V., Nancy S., Pop I. (2011). Double-diffusive convection from a permeable vertical surface under convective boundary condition. *International Communications in Heat and Mass Transfer*, Vol. 38, pp. 1183-1188.
<https://doi.org/10.1016/j.icheatmasstransfer.2011.06.006>

Turkyilmazoglu M. (2013). The analytical solution of mixed convection heat transfer and fluid flow of a MHD viscoelastic fluid over a permeable stretching surface. *International Journal of Mechanical Sciences*, Vol. 77, pp. 263-268.
<https://doi.org/10.1016/j.ijmecsci.2013.10.011>

Yadav D., Kim C., Lee J., Cho H. H. (2015). Influence of magnetic field on the onset of nanofluid convection induced by purely internal heating. *Computers and Fluids*, Vol. 121, pp. 26-36. <https://doi.org/10.1016/j.compfluid.2015.07.024>

Nomenclature

u, v	velocity components in x and y directions respectively
x, y	co-ordinates along and normal to the plate
c	constant
k	thermal conductivity
C_∞	ambient solutal concentration
C	solutal concentration
ϕ_w	nanoparticle volume fraction at the wall
S	dimensionless concentration
ϕ	nanoparticle volume fraction
ϕ_∞	ambient nanoparticle volume fraction
Bi	Biot number
M	magnetic parameter
g	acceleration due to gravity
S_1	internal heat generation/absorption
Pr	Prandtl number
Le	Lewis number
Gr_x	local Grashof number
Nu_x	local Nusselt number
Nb	Brownian motion parameter
D_B	coefficient of Brownian diffusivity
D_T	thermophoretic diffusion coefficient
h_f	convective heat transfer coefficient
D_s	solutal diffusivity
D_{CT}	Soret diffusivity
a_m	thermal diffusivity
Nc	regular buoyancy ratio

Nr	nanoparticle buoyancy ratio
Nt	thermophoresis parameter
η	similarity variables
λ	mixed convection parameter
μ	dynamic viscosity
ν	kinematic viscosity
β_T	volumetric thermal expansion coefficient
β_C	volumetric solutal expansion coefficient
ψ	stream function
f	dimensionless stream function
T	temperature
θ	dimensionless temperature
T_f	temperature of the hot fluid
ρ	density of the fluid
T_∞	ambient temperature
$\rho_{f\infty}$	density of the base fluid
u_∞	characteristics velocity
ρ_p	mass density of the nanoparticle
S_T	Soret number
τ_w	shear stress at the wall
Ec	Eckert number
Q	heat source/sink parameter
R	radiation parameter
Kp	porosity parameter
Sc	Schmidt number
$(\rho c)_f$	heat capacity of the fluid
Re_x	local Reynolds number
$(\rho c)_p$	effective heat capacity of the nanoparticle
NSH_x	local nanoparticle Sherwood number
Sh_x	local Sherwood number
q_n	mass flux of nanoparticle at the wall
q_m	regular mass flux at the wall
q_w	heat flux at the wall
J	ratio between the effective heat capacity of the nanoparticle material and heat capacity of the fluid

Subscripts

w	wall condition
∞	ambient condition
C	concentration
T	temperature

